Experimental Behavior and Design-Oriented Analysis of Sandwich Beams with Bio-based Composite Facings and Foam Cores

Dillon Betts[1] S.M.ASCE, Pedram Sadeghian[2] M.ASCE, and Amir Fam[3] F.ASCE

ABSTRACT: In this paper, sandwich beams made of bio-based fiber-reinforced polymer (FRP) composite facings and foam cores were studied. The FRP facings consisted of a plant-based bidirectional flax fiber fabric (400 g/m^2) and a bio-based epoxy resin (30% bio content) and the foam cores were made of 75 mm thick closed cell polyisocyanurate. A total of nine sandwich beam specimens (1200 mm long and 150 mm wide) were prepared and tested under three-point bending. The parameters of the study were core density (32, 64, and 96 kg/m^3) and facing thickness (one, two, and three layers of flax fabric). Three failure mechanisms were observed during testing, including: top face wrinkling/crushing, core shear, tensile rupture of bottom face. It was shown that the foam with the density of 96 kg/m^3 is stiff and strong enough to achieve the tensile rupture of the flax FRP (FFRP) facing. Also, a nonlinear behavior was observed for the sandwich beams. A bilinear stress-strain model for FFRP facing was proposed and, based on that, closed-form moment-curvature and load-deflection equations of the sandwich beams were derived for design applications. The proposed design-oriented model was verified against the test data of this study and an independent study capturing the stiffness, strength, and nonlinearity of the test specimens.

KEYWORDS: Sandwich, Composite, Flax, Bio-based, Nonlinear, Failure modes, Design.

---

[1] PhD Student, Department of Civil and Resource Engineering, Dalhousie University, 1360 Barrington Street, Halifax, NS B3H 4R2, Canada. Email: dillonbetts@dal.ca

[2] Assistant Professor and Canada Research Chair in Sustainable Infrastructure, Department of Civil and Resource Engineering, Dalhousie University, 1360 Barrington Street, Halifax, NS, B3H 4R2, Canada. Email: pedram.sadeghian@dal.ca (corresponding author)

[3] Donald and Sarah Munro Chair Professor in Engineering and Applied Science and Associate Dean (Research and Graduate Studies), Department of Civil Engineering, Queen's University, Kingston, ON, K7L 3N6, Canada. Email: amir.fam@queensu.ca

INTRODUCTION

Sandwich panels are often used in applications where light weight and/or insulation efficiency are required. They have high flexural strength as the lightweight core separates the strong facings apart, thereby providing a large moment of inertia to resist bending (Allen 1969). As fiber-reinforced polymer (FRP) composites have relatively high specific strengths, they are a popular choice for facing materials. However, due to the relatively low strength of typical core materials, the core often governs the failure mechanism and the FRP facings rarely reach their full tensile strength. As such, the high strength of the FRP facings is often not utilized (Fam et al., 2016; Sadeghian et al., 2016). This phenomenon presents an opportunity to use natural fibers (e.g. flax) with lower strength, which are more environmentally friendly, as alternatives to synthetic fibers. Moreover, thermoset resins with high bio-content can be used to make the FRP facings more environmentally friendly. Flax FRP (FFRP) composites represent a sustainable option with a lower embodied energy than traditional fibers such as glass or carbon (Mak and Fam, 2016).

Behavior of sandwich structures, in general, has been studied extensively since the mid-20th century. Allen (1969) presented fundamental approaches for the analysis of sandwich panels using the ordinary beam theory. For ease of calculation, Allen's text provides a simplified analysis which produces moderately accurate results. In the early 1990s, researchers began to use high-order analyses to model the behavior of sandwich panels, in order to achieve more accurate results (Frostig et al., 1992; Frostig and Baruch, 1996; Thomsen and Rits, 1998). The high-order theory presented by Frostig et al. (1992) improves upon the method presented by Allen (1969) by accounting for the nonlinearity of the transverse and longitudinal deflections of the core material. Finite element modelling of sandwich panels has also been used. Sharaf and Fam (2012) developed a finite element model for the analysis of sandwich panels with soft cores and glass FRP (GRFP) facings. The model

is able to predict flexural behavior and failure modes. Fam et al. (2016) developed a semi-analytical model to predict behavior of sandwich panels constructed of polyurethane foam cores and GFRP facings under flexural loading. This model accounts for nonlinear properties of the foam cores and the GFRP facing properties and was validated with experimental testing.

The use of natural fibers and bio-based resins for facings of sandwich panels in civil applications has been studied in the recent past under flexural (Mak et al., 2015; Sadeghian et al., 2016) and axial loads (Codyre et al., 2016). However, the studies were only experimental and used unidirectional FFRP sheets for the facings. The experimental database for bio-based sandwich panels remains extremely limited. There is a gap regarding bidirectional FFRPs providing two-way behavior as expected for many wall and roof panels. Additionally, because of the complex behavior of sandwich panels in combined flexural and shear loading and the wide variety of failure modes, the currently available analytical models are quite sophisticated and require very advanced knowledge in mathematics and computer programming. No simple design-oriented models are available for structural engineering applications of sandwich panels. This paper aims to fill the several gaps stated above using an experimental program and a design-oriented analytical modeling.

EXPERIMENTAL PROGRAM

Test Matrix

Nine sandwich beam specimens were fabricated and tested under three-point bending. The specimens were comprised of FFRP facings and closed cell polyisocyanurate foam cores with a thickness of 75 mm. The test parameters were facing thickness and foam core density. Three facing thicknesses (1, 2 and 3 layers of flax fabric) and three core densities (32, 64, and 96 kg/m^3) were compared. The parameters were chosen such that different failure modes could be examined. The test matrix is shown

in Table 1. The specimens were identified according to the core type and number of flax layers as per the following convention: XFL-CY, where X is the number of flax layers (i.e. 1, 2, or 3) and Y is the nominal core density in kg/m^3 (i.e. 32, 64, or 96). For example, 2FL-C64 indicates a sandwich specimen with 2 flax layers at either side of a core with a density of 64 kg/m^3.

Materials

For the facings, a balanced bidirectional flax fiber fabric (2x2 twill) was used with a bio-based epoxy resin. The fabric had a reported nominal areal mass of 400 g/m^2 (gsm) which was measured to be 410 gsm. For the resin, a bio-based epoxy was used. This resin is typically used with a fast setting hardener, however, for this experiment a longer pot life was required and a different hardener was used. The reported technical data from the manufacturer is approximate as it assumes the use of the fast setting hardener. When mixed with the fast setting hardener, the resin has a reported tensile strength, modulus and elongation of 53.2 MPa, 2.65 GPa, and 6%, respectively. It has an approximate bio-based carbon content of 30% after mixing. In order to determine the properties of the epoxy, five identical dumbbell-shape coupon specimens were fabricated and tested in accordance with ASTM D638 (ASTM 2013). The tests showed that the average and standard deviation (SD) of the tensile strength, Young's modulus and ultimate strain were 57.9 ± 0.4 MPa, 3.20 ± 0.13 GPa, and 0.0287 ± 0.0018 mm/mm, respectively.

The mechanical properties of the facing FFRP were determined through compression and tension coupon testing. A uniaxial tension test was performed on five identical FFRP specimens fabricated using the materials cited above as per ASTM D3039 (ASTM 2014). The specimens were 250 mm long, 25 mm wide, and two plies thick. The specimens had 62.5 mm long FFRP tabs on each end, which were adhered to the specimen using the bio-based resin. The specimens were tested in uniaxial tension at a rate of 2 mm/min. The results (average ± SD) of these tests show that the facing

composites have a tensile strength, initial tensile modulus, and ultimate strain of 45.4 ± 1.8 MPa, 7.51 ± 0.69 GPa and 0.0083 ± 0.0009 mm/mm, respectively. The stress-strain plot of each test specimen is shown in Figure 1.

Five identical compression coupon specimens were also tested. Due to the unavailability of the testing apparatus with hydraulic grips for standard test method in compression, an alternative test was developed to evaluate the FFRP strength. Compression specimens were manufactured by laminating eight two-ply composite strips together using the same bio-epoxy. The ends were fixed into a square aluminum cap (38 mm wide and 18 mm deep) using a fast curing adhesive. The specimens were 70 mm long, 25 mm wide and 25 mm thick. Strain gauges were applied at the center of both sides in the longitudinal direction. The specimens were tested in uniaxial compression at a rate of 0.5 mm/min. The results (average ± SD) show that the facing composites have an initial compressive modulus of 6.73 ± 1.59 GPa and a compressive strength and corresponding strain of 86.4 ± 2.2 MPa and 0.0327 ± 0.0010 mm/mm, respectively. The stress-strain plots and typical test specimens are shown in Figure 1. During the tests, the strain in the specimens exceeded the capacity of the strain gauges. Therefore, to show the rest of the stress-strain curve, the stroke was converted to strain and calibrated using the available strain gauge data. This portion of the plot is shown in Figure 1 as a dashed grey line.

As shown in Figure 1, the coupons made of bidirectional flax fabric exhibit a nonlinear behavior. The nonlinearity of composites made of natural fibers have been reported, previously (Christian and Billington, 2011; Yan et al., 2012; Mak et al., 2014; Mathura and Cree, 2016; and Hristozov et al., 2016). In this study, the stress-strain behavior of the FFRPs is modelled as a bilinear plot with a point of transition (POT) at a strain of 0.0018 mm/mm. The primary modulus was determined by finding the slope of the stress-strain diagram between strains of zero and 0.0018

mm/mm. As shown in Figure 1, the secondary modulus was defined as the slope of a chord passing through a strain of 0.0018 mm/mm and the ultimate strain. From the compression and tension tests, the secondary tensile modulus and secondary compression modulus were found to be 4.59 ± 0.37 GPa and 2.36 ± 0.19 GPa, respectively.

Each specimen had a core made of a closed cell polyisocyanurate foam. Three different densities were used: 32 kg/m^3, 64 kg/m^3 and 96 kg/m^3. The actual densities have been measured as 31.2 kg/m^3, 62.4 kg/m^3 and 91.7 kg/m^3, respectively (Codyre et al., 2016). Each foam type was received in sheets, 1200 mm wide, 2400 mm long and 75 mm thick. The moduli and strengths of each foam as given by the manufacturer are shown in Table 2.

Specimen Fabrication

The fabrication process is shown in Figure 2. A 600 mm x 1200 mm section of the foam was cut from a 1200 mm x 2400 mm foam board. The foam surface was then cleaned of all dust and debris. Once the epoxy and hardener were mixed, a layer of resin was applied to the top surface of the foam. A section of flax fiber fabric 600 mm wide and 1200 mm long was then placed on the foam with its warp direction fibers oriented parallel to the longitudinal axis of the specimen. Additional resin was applied on the fabric. This was repeated as required depending on the specimen's facing thickness. To create a clean finish, parchment paper was placed on the top surface and a steel roller was used to remove air and excess resin. A weighted flat board was then placed on the section and the resin was allowed to cure for a minimum of seven days. This process was repeated on the other side of the panel to complete the opposite facing. After both sides of a section were cured, the specimens were cut to their final size of 150 mm wide and 1200 mm long using a band saw and stored in a dry environment until testing.

Test Setup and Instrumentation

Each specimen was tested under three-point bending using a 1 MN actuator that applied the load to the specimen at a rate of 8 mm/min through a 150x150x225 mm Hollow Structural Section (HSS) as shown in Figure 3. The HSS was used to avoid local failure and to ensure an even distribution of the load. A 25-mm diameter hole was cut into the bottom face of the HSS such that a strain gauge with a 6 mm gauge length could be installed at the center of the top FFRP facing. Another strain gauge was also installed at the center of the bottom facing. Both strain gauges were installed to measure longitudinal strains. Two displacement transducers were placed at mid-span, 10 mm from each edge, to measure deflection. As shown in the test set-up schematic in Figure 3, one support was a roller, while the other was a hinge. A data acquisition system recorded the force, stroke, displacement and strains at a rate of six samples per second.

EXPERIMENTAL RESULTS AND DISCUSSIONS

The main test results are load-deflection, and load-facings strain, and moment-curvature responses of the sandwich beam specimens. Table 3 presents the test results of each specimen, including: the peak load (P_u) and corresponding deflection (δ_u), the peak moment (M_u), the initial stiffness (K), the initial flexural rigidity (EI), and the failure mode. The initial stiffness was taken as the first linear slope of the load-deflection plot and the initial flexural rigidity was determined likewise using the moment-curvature plot. The following sections present the various observations and test results, including failure modes and the effect of facing thickness and core density on the moment-curvature and load-deflection diagrams.

Failure Modes

Sandwich panels are susceptible to several types of failure. In this study, four failure modes were observed: compression face wrinkling (CW), compression face crushing (CC), tensile face rupture

(TR), and core shear failure (CS). The failure mode for each specimen is presented in Table 3 and a photo of each failure mode is also shown in Figure 4. For the specimens with facings containing only one layer of flax fabric, the compression facing governed failure in both 1FL-C32 and 1FL-C64, whereas the tension face of 1FL-C96 controlled failure. As compression face wrinkling is dependent on the core strength (Allen 1969), the two weaker core specimens exhibit face wrinkling, whereas the strongest core result in a tensile facing failure.

Specimens 2FL-C32 and 2FL-C64 with two-layer facings show compression wrinkling and shear type failure mechanisms. As the facing strength is approximately double that of the 1FL specimens, it is not surprising that failure mode would shift to a core type failure. On the other hand, the 2FL-C96 specimen failed in tensile rupture due to the higher shear strength of the core. Looking at the failure of the 3FL-C32 and 3FL-C64 specimens with three-layer facings, it is clear that the core material controlled failure, as in both cases the failure was in pure shear, completely independent of the facing materials. Specimen 3FL-C96 failed simultaneously by facing tensile rupture and core shear, referred to herein as a balanced condition. Generally, as the foam core density and facing thickness increase, the peak loads and the corresponding deflections also increase. Typically, the lower density foams (C32 and C64) govern the failure mode, while the FFRP facings govern the failure mode for the C96 specimens.

Effect of Facing Thickness

Figure 4 shows the effect of facing thicknesses on the load-deflection diagrams for the different core densities. The deflection used to make these plots was taken as the average from the two displacement transducers. For each foam density, the peak load and initial stiffness increase with facing thickness. For example, by looking at the 32 kg/m^3 foam cores, when the facing thickness increases from one to two layers of flax (i.e. from 1FL-C32 to 2FL-C32), the peak load and initial stiffness increase by 79%

and 36%, respectively. Looking at the failure modes (in the same figure), it can be seen that the failure mode progresses from facing-controlled failure (compression crushing/wrinkling) to a core controlled failure (wrinkling/shear).

Figure 5 shows the effect of facing thickness on the moment-curvature and load-strain diagrams for each foam density. The measured curvature, ψ, is based on the top face strain, ϵ_t, the bottom face strain, ϵ_b, and the specimen height, h, and was calculated using Eq. 1. As expected, the peak moment and initial rigidity increased with facing thickness. For example, moving from 1FL-C32 to 2FL-C32, the increases in moment and rigidity (i.e. the initial slope of the moment-curvature diagram) were 79% and 116%, respectively.

$$\Psi = \frac{\epsilon_t + \epsilon_b}{h} \tag{1}$$

Effect of Core Density

The core density has a major impact on the failure mode of these sandwich panels. The beam stiffness is greatly affected by the core density whereas it has little effect on the initial flexural rigidity, EI, as the facings provide the bending stiffness of the member. For example, looking at the difference between 1FL-C32 and 1FL-C64, the initial stiffness is increased by 87%, whereas the initial flexural rigidity is only increased by 23%. This difference could be explained by the fact that shear deformation influences the load-deflection behavior of the specimens, but does not affect the moment-curvature behavior. This is also accounted for in the design-oriented model as discussed in a subsequent section. The change in core density had a major impact on the ultimate moment at the peak load observed, but little effect on the rigidity as indicated before. For example, looking again at the difference between 1FL-C32 and 1FL-C64, the increase in peak moment is 81%, whereas the increase in rigidity is only 23%.

ANALYTICAL STUDY

Simplified models were developed for the calculation of the moment-curvature and load-deflection behavior of sandwich panels constructed of foam cores and FFRP facings. The models were verified with the data presented in this study as well as data presented by Mak et al. (2015) and were then expanded to develop a simple design procedure which could be used by designers.

Moment-Curvature Behavior

As noted by numerous researchers, FFRPs display a bilinear stress-strain behavior (Bensadoun et al., 2016; Mak et al., 2015; Sadeghian et al., 2016; Hristozov et al., 2016). This is also evident when examining the stress-strain curves shown in Figure 1. As a result, the moment-curvature behavior of the sandwich panels could also be approximated as bilinear. Figure 6(a) shows the cross-section of a panel and Figure 6(b) shows the bilinear models used in developing the analytical model.

Assumptions

The following assumptions were made to develop the simplified moment-curvature model:

a) The moment resistance provided by the foam is negligible when compared to the resistance of the FFRP facings. This assumption is based on the extremely small values of Young's modulus of the core (shown in Table 2), compared to the facings.
b) The secondary tensile modulus is approximately two thirds of the initial tensile modulus (Wroblewski et al., 2016) and the secondary compression modulus is approximately two fifths of the initial compression modulus. These assumptions are established based on the measured stress-strain curves in Figure 1. Conservatively, the modulus used in the failure mode equations, presented later, is based on these secondary moduli, as shown in Equation 3.

c) The neutral axis is located at the center of the cross section. Figure 8 shows a diagram of the neutral axis (established from top and bottom longitudinal strain measurements) versus moment, which justifies this assumption. This also means that the moduli used in the moment-curvature model can be approximated as the average of the compression and tensile moduli, which were determined through testing. Therefore, the moduli are taken as shown in Equations 2 and 3, where E_{ft} and E_{fc} are the primary tensile modulus and the primary compression modulus, respectively.

$$E_{f_1} = \frac{1}{2}(E_{f_t} + E_{f_c}) \tag{2}$$

$$E_{f_2} = \frac{1}{2}(\frac{2}{3}E_{f_t} + \frac{2}{5}E_{f_c}) = \frac{1}{3}E_{f_t} + \frac{1}{5}E_{f_c} \tag{3}$$

Analysis Procedure

The bilinear model requires the calculation of the coordinates of two points in terms of moment and curvature: the point of transition (POT) at the end of the first slope (M_o, Ψ_o), and a 'hypothetical' ultimate point at the end of the second slope (M_u, Ψ_u). The reason for referring to the ultimate point as 'hypothetical' is because it is based on the ultimate failure strain of the facing which may never be reached (for example due to core shear or wrinkling, which will be considered later). The calculations are based on the strain developed in the facings. The POT strain, ϵ_{fo}, is a material property that can be determined from the stress-strain plots of the facing material. As shown in Figure 6(b), the ultimate strain of the facing material, ϵ_{fu}, is based on the ultimate tensile strength of the facing material, f_{fu}, the stress at the material POT, f_{fo}, and the secondary modulus of the material, E_{f2} and is determined by Equation 4.

$$\epsilon_{f_u} = \epsilon_{f_o} + \frac{f_{fu} - f_{f0}}{E_{f2}} \tag{4}$$

The calculation of both the POT moment and the 'hypothetical' ultimate moment are based on the geometrical and material properties of the specimens, as given by:

$$M_0 = tbdE_{f_1}\epsilon_{f_0} \tag{5}$$

$$M_u = tbd[E_{f_1}\epsilon_{f_0} - E_{f_2}(\epsilon_{f_u} - \epsilon_{f_0})] \tag{6}$$

where t is the facing thickness, b is the specimen width, and d is the distance between the centroids of the top and bottom facings. The curvatures at the POT and ultimate points are calculated using Equations 7 and 8.

$$\Psi_0 = \frac{2}{d}\epsilon_{f_0} \tag{7}$$

$$\Psi_u = \frac{2}{d}\epsilon_{f_u} \tag{8}$$

As shown in Figure 6(b), the bilinear response established up to the 'hypothetical' ultimate moment M_u may be terminated at a lower load level based on the various failure criteria. The model prediction for each test specimen is shown in Figure 5, after implementing the proper failure criteria predicted for each case (discussed later). These moment-curvature diagrams will be used to determine the load-deflection diagrams required to complete the analysis.

Load-Deflection Behavior

The load-deflection model was developed by superimposing both bending and shear deformations of three-point loading as shown in Figure 8(a). The bending deformation (Δ_B) was derived by integration of curvature over the length of the beam using the moment-area method ($\Delta_B=\Sigma A_i X_i$), where A_i is the area of each segment under curvature diagram over the half length of the beam and X_i is the distance from the centroid of each segment to the end of the beam as shown in Figure 8(a). The major assumption in the load-deflection model is a bilinear behavior that follows the bilinear behavior of the moment-curvature diagrams. The primary and secondary slopes are based on the loads

corresponding to the POT moment, M_0, and the ultimate moment, M_u, and are determined by Equations 9 and 10.

$$P_0 = \frac{4}{L} M_0 \tag{9}$$

$$P_u = \frac{4}{L} M_u \tag{10}$$

The equations for the deflections at the POT and ultimate load were developed based on curvatures as shown in Figure 7. Then, the equations were modified to include the contribution of core shear deflection ($\Delta_V = VL_a/G_cA_v$), where V is the shear force over the shear span L_a, G_c is the core shear modulus, and A_v is the shear area. The equations for the POT and ultimate deflections are given in Equations 11 and 12, respectively.

$$\Delta_0 = \frac{L^2}{6d}\epsilon_{f_o} + \frac{P_0 L}{4G_c(\frac{bd^2}{c})} \tag{11}$$

$$\Delta_U = \frac{L^2}{12d}\left[(1+\lambda)\epsilon_{f_0} + \left(2-\lambda-\lambda^2\right)\epsilon_{f_u}\right] + \frac{P_U L}{4G_c(\frac{bd^2}{c})} \tag{12}$$

$$\lambda = \frac{1}{2 + 2\frac{E_{f_2}}{E_{f_1}}\left(\frac{\epsilon_{fu}}{\epsilon_{f_0}} - 1\right)} \tag{13}$$

After determining the ultimate deflection due to shear and moment, the curve is truncated by implementing the failure criteria as presented in the next section. It should be highlighted that Equations 11 and 12 were derived for three-point bending loading. The equations can be easily modified for the case of four-point bending as presented in Figure 8(b) and other loading conditions.

Ultimate Conditions Prediction

The moment-curvature and load-deflection models presented are based on the ultimate strength of the facings. Therefore, the models as they are would be adequate for predicting the ultimate load capacity

for the cases of compression face crushing or tensile face rupture failure modes. However, as previously discussed, sandwich panels are susceptible to several failure modes, and as such, additional failure criteria are required.

Failure Criteria

The range possible failure modes are: (i) compression face wrinkling, (ii) tension face rupture, (iii) core shear failure and (iv) compression face crushing. The failure loads for failure modes (i), (ii) and (iii) can be determined by the equations developed by Triantafillou and Gibson (1987), which are presented as Equations 14, 15 and 16, respectively:

$$P_{CW} = 0.57\, C_1 C_3^{2/3} E_f^{1/3} E_s^{2/3} (\rho_c/\rho_s)^{2A/3}\, bc\frac{t}{L} \tag{14}$$

$$P_{TR} = C_1 \sigma_{ft} bc\frac{t}{L} \tag{15}$$

$$P_{CS} = \frac{C_4(\rho_c/\rho_s)^B \sigma_{sy} bc}{\sqrt{\left(\frac{C_3(\rho_c/\rho_s)^A E_s}{2C_1\frac{t}{L}E_f}\right)^2 + \left(\frac{1}{C_2}\right)^2}} \tag{16}$$

where P_{CW}, P_{TR}, and P_{CS} are the failure loads for compression face wrinkling, tensile face rupture, and core shear failure, respectively. C_1 and C_2 are constants depending on the loading arrangement; for three-point bending they are taken as 4 and 2, respectively. A, B, C_3, and C_4 are constants depending on the relative core density, the relative core modulus, and the relative core strength (Triantafillou and Gibson, 1987). These values are determined by relating the density, modulus and strength of each core to the values of the material from which the core was foamed. That is, the relative core density, relative core modulus and relative core strength are represented as (ρ_c/ρ_s), (E_c/E_s) and (τ_c/σ_s), respectively. A, B, C_3, and C_4 were found to be 1.52, 1.24, 0.75 and 0.10, respectively by plotting (ρ_c/ρ_s) *vs.* (E_c/E_s) and (ρ_c/ρ_s) *vs.* (τ_c/σ_s) and using Equations 17 and 18.

$$\left(\frac{E_c}{E_s}\right) = C_3 \left(\frac{\rho_c}{\rho_s}\right)^A \quad (17)$$

$$\left(\frac{\tau_c}{\sigma_s}\right) = C_4 \left(\frac{\rho_c}{\rho_s}\right)^B \quad (18)$$

As was proposed by Triantafillou and Gibson (1987), the failure mode map developed in this study is based on the interface between these three failure modes and therefore does not account for compression crushing (iv). Since the ultimate compressive strength of FFRP skin is double that of its tensile strength (Figure 1), facing crushing without (iv) wrinkling will not govern. In this study, failure models developed by Triantafillou and Gibson (1987) will be used.

Failure Mode Maps

To predict the failure mode of the sandwich panels, a failure mode map was developed in the Matlab programming language based on the equations presented by Triantafillou and Gibson (1987) and is shown in Figure 9 for the loading case discussed in this paper. The failure mode maps will be beneficial for the design of these sandwich panels as they can be used to ensure a desired failure mode or provide the minimum design parameters for a design load. Also shown on this map are specimens 1 to 9 based on their geometric and relative density properties represented by the horizontal and vertical axes. It can be seen that the specimens land in various regions representing the three predicted primary failure modes. It can also be seen that specimen 6 lies on the border line between two regions.

Verification

Table 3 shows the properties of the test specimens and the results of the model. Figures 4 and 5 show the verification of the load-deflection and moment-curvature models. These figures show the comparison of the models for different facing thicknesses for each foam type. In specimen 2FL-C64, the ultimate moment and peak load were both overestimated by 48%. This error is introduced through the failure equations used to predict these ultimate capacities. For the same specimen, the new models

predicted the initial stiffness and initial rigidity to within 16% and 20%, respectively. This was the only specimen for which these values were overestimated, for all other specimens, the models predicted under the actual values. This could be due to the fact, that due to an error in the test set-up for the 2FL-C64 specimen, both supports were hinge type supports. There is the potential that this caused an axial compression load in the specimen which could have caused premature failure. The average differences of the initial stiffness and rigidity between the model and the test results were -13% and -15%, respectively.

The model has also been verified using data of specimens tested by Mak et al. (2015) as shown in Figure 10. In the study by Mak et al. (2015) a number of different specimens were tested. The FE-V type specimens were chosen for verification as they were fabricated using unidirectional FFRP faces which were made by using vacuum bags which differs from the wet lay-up method used in the current study. Because the study by Mak et al. (2015) was four-point bending, the model had to be adjusted to accommodate this difference. This adjustment is shown alongside the original model development in Figure 7. The results imply that the proposed bilinear models are applicable for predicting behavior of sandwich beams with foam cores and FRP facing made of both unidirectional and bidirectional flax fabrics.

Design Procedure and Example

Based on the failure mode maps, the load-deflection and moment-curvature models, a simple design procedure was developed for sandwich panels with FFRP facings and soft foam cores. The design procedure is shown in the form of a flow chart in Figure 11. Given a factored design load, the preliminary design variables (i.e. the FFRP facing thickness and core density) can be obtained using the failure mode map. This can be used to dictate the failure mode or to determine the minimum allowance for the design variables. With the known facing thickness and core density, the designer

can develop the load-deflection and moment-curvature plots, as well as the exact failure load as the minimum calculated from Equations 14, 15 and 16. The deflection limit criteria for serviceability can then be checked, and if necessary, the design can be updated (for example by increasing core thickness or density or facing thickness) to satisfy the required deflection limits. It should be noted that as this design procedure has been developed with limited test data, more research is required in this area. This research should include tests on panels with different core densities, different face thicknesses, different polymer types and different fabric configurations. As the proposed models used in this design procedure have already been shown as applicable for use with data from an independent study (Mak et al. 2015), this procedure warrants further investigation.

As an example of how to use the proposed design procedure, let us assume that a sandwich panel constructed of FFRP facings and foam core needs to be designed for a span length of 1100 mm and is required to support a factored concentrated load of 6 kN applied at its mid-span. Referring to Figure 9, it can be seen that to resist 6 kN, the minimum values of t/L of 0.003 and ρ_c/ρ_s of 0.05 would be required. Knowing the span length of 1100 mm and the density and elastic modulus of the unfoamed core material of 1200 kg/m^3 and 1600 MPa, respectively, we can determine that the minimum required facing thickness and foamed core density would be 3.3 mm and 60 kg/m^3, respectively. This point happens to be in the Tension failure region of the failure mode map, however, each failure load (Equations 14 to 16) should be calculated and the minimum value should be considered to govern. Taking E_f as E_{f2}, we can determine the failure loads P_{cw}=6.54 kN, P_{TR}=6.23 kN, and P_{CS}=7.10 kN using Equations 14, 15 and 16, respectively. As expected, the tensile rupture failure load, P_{TR}, governs, which agrees with the failure map observation. To ensure that this failure load is reached, a relative core density equal to or exceeding 0.05 (therefore, for a material with an unfoamed

density of 1200 kg/m^3, a foam density of 60 kg/m^3) must be selected along with a facing thickness equal to or exceeding 3.3 mm. Therefore, three layers of FFRP and the C64 type foam are required.

At this point, the load-deflection and moment-curvature model would need to be developed using the procedure outlined earlier. For this example, the models are shown in Figures 4 and 5. Assuming that the load was factored using a factor of 1.4, the service load in this problem would be approximately 4.3 kN. Looking at the load-deflection model, a 3FL-C64 sandwich panel has a deflection of approximately 32 mm at a load 4.3 kN. Based on the simplicity of this example and assuming that the failure mode maps for these types of sandwich panels were readily available to practicing engineers, this design procedure could be economically feasible for use in industry. Alternatively, designers could develop the failure maps using Equations 14, 15 and 16, relatively easily.

CONCLUSIONS

In this study, nine sandwich beams were constructed using FRPs comprised of bidirectional flax fabrics and bio-based epoxy resin for the facings and a polyisocyanurate foam for the core. The specimens were tested under three-point bending. Based on the test data, it can be concluded that the facings provide the majority of the flexural strength of the sandwich beams. Also, the C96 (96 kg/m^3 density) type foam is stiff enough that a balanced design can be achieved using FFRP facings. The balanced design is defined here as a simultaneous material failure, where the tension facing fails by tensile rupture while the foam core simultaneously fails by shear (i.e. both materials reach their full potential strengths). Increasing the facing thickness creates a change in the failure mode, moving from a facing-controlled failure to a core-controlled failure. Using the established material test data, moment-curvature and load-deflection models were developed and compared with the experimental

results of the panels. A failure mode map was established for the tested panels and a simple design procedure was developed. The design procedure is simple enough that it could be easily used by designers. A design example using this procedure was presented. The proposed bilinear models and design-oriented analysis are applicable for analysis and design of sandwich beams with foam cores and FRP facings made of both unidirectional and bidirectional flax fabrics. Future work in this research area should include the development of appropriate safety factors for design and further testing and analysis of sandwich panels with FFRP facings.

1. ACKNOWLEDGEMENTS

Authors would like to thank Blair Nickerson, Jesse Keane, Brian Liekens, and Brian Kennedy for their assistance in the lab. The authors would also like to acknowledge and thank Bioindustrial Innovation Canada (BIC), Queen's University, and Dalhousie University for their in kind and financial support.

2. REFERENCES

Allen, H. G. (1969). *Analysis and Structural Design of Sandwich Panels*. Pergamon Press, Oxford, UK.

ASTM. (2013). "ASTM D638, Standard test method for tensile properties of plastics." *Annual Book of ASTM Standards*.

ASTM. (2014). "ASTM D3039, Standard test method for tensile properties of polymer matrix composite materials." *Annual Book of ASTM Standards*.

Bensadoun, F., Vallons, K. A. M., Lessard, L. B., Verpoest, I., and Van Vuure, A. W. (2016). "Fatigue behaviour assessment of flax-epoxy composites." *Composites Part A: Applied*

Science and Manufacturing, Elsevier Ltd, 82, 253–266.

Codyre, L., Mak, K., and Fam, A. (2016). "Flexural and axial behaviour of sandwich panels with bio-based flax fibre-reinforced polymer skins and various foam core densities." *Journal of Sandwich Structures and Materials*, 1–22.

Fam, A., Sharaf, T., and Sadeghian, P. (2016). "Fiber element model of sandwich panels with soft cores and composite skins in bending considering large shear deformations and localized skin wrinkling." *Journal of Engineering Mechanics*, 142(5), 1–14.

Frostig, B. Y., Baruch, M., Vilnay, O., and Sheinman, I. (1992). "High-order theory for sandwich-beam behavior with transversely flexible core." *Journal of Engineering Mechanics*, 118(5), 1026–1043.

Frostig, Y., and Baruch, M. (1996). "Localized Load Effects in High-Order Bending of Sandwich Panels with Flexible Core." *Journal of Engineering Mechanics*, 122(11), 1069–1076.

Hristozov, D., Wroblewski, L., and Sadeghian, P. (2016). "Long-term tensile properties of natural fibre-reinforced polymer composites: Comparison of flax and glass fibres." *Composites Part B: Engineering*, Elsevier Ltd, 95, 82–95.

Mak, K., and Fam, A. (2016). "Bio Resins and Bio Fibers for FRP Applications in Structural Engineering Applications." *7th International Conference on Advanced Composite Materials in Bridges and Structures*, Canadian Society for Civil Engineering, Vancouver, BC, Canada, 1–6.

Mak, K., Fam, A., Asce, M., and Macdougall, C. (2015). "Flexural Behavior of Sandwich Panels with Bio-FRP Skins Made of Flax Fibers and Epoxidized Pine-Oil Resin." *Journal of Composites for Construction*, 19(2003), 1–13.

Sadeghian, P., Hristozov, D., and Wroblewski, L. (2018). "Experimental and analytical behavior of sandwich composite beams: Comparison of natural and synthetic materials." *Journal of*

Sandwich Structures and Materials, 20(3), 287–307.

Sharaf, T., and Fam, a. (2012). "Numerical modelling of sandwich panels with soft core and different rib configurations." *Journal of Reinforced Plastics and Composites*, 31(11), 771–784.

Thomsen, O. T., and Rits, W. (1998). "Analysis and design of sandwich plates with inserts—a high-order sandwich plate theory approach." *Composites Part B: Engineering*, 29(6), 795–807.

Triantafillou, T. C., and Gibson, L. J. (1987). "Failure Mode Maps for Foam-Core Sandwich Beams." *Materials Science and Engineering*, 95, 37–53.

Wroblewski, L., Hristozov, D., and Sadeghian, P. (2016). "Durability of bond between concrete beams and FRP composites made of flax and glass fibers." *Construction and Building Materials*, Elsevier Ltd, 126, 800–811.

Table 1: Test matrix.

No.	Specimen I.D.	Number of FFRP layers in each facing	Nominal core density (kg/m^3)
1	1FL-C32	1	32
2	2FL-C32	2	32
3	3FL-C32	3	32
4	1FL-C64	1	64
5	2FL-C64	2	64
6	3FL-C64	3	64
7	1FL-C96	1	96
8	2FL-C96	2	96
9	3FL-C96	3	96

Table 2: Mechanical properties of foam cores.

Foam type	Parallel to rise						Perpendicular to rise					
	E_c	E_t	G	f_{cu}	f_{tu}	τ_u	E_c	E_t	G	f_{cu}	f_{tu}	τ_u
C32	4 823	8 268	2 067	186	248	172	2 302	3 190	1 515	124	179	124
C64	14 469	18 603	5 856	585	551	379	9 646	10 748	5 167	427	406	344
C96	32 865	27 146	7 234	978	930	585	21 290	15 709	6 063	834	792	489

Note 1. Data is presented in kPa.

Note 2. E_c = compressive modulus, E_t = tensile modulus, G = shear modulus, f_{cu} = compressive strength, f_{tu} = tensile strength, and τ_u = shear strength.

Table 3: Summary of experimental and analytical results.

		Peak load (kN)			Deflection at peak load (mm)			Initial stiffness (N/mm)			Peak moment (kN-m)			Initial rigidity, EI (kN-m^2)			Failure mode	
No.	Specimen	Test	Model	Err.	Test	Model	Err.	Test	Model	Err.	Test	Model	%	Test	Model	Err.	Test	Model
1	1FL-C32	1.31	1.31	0%	29.49	30.43	3%	54.00	49.58	-8%	0.36	0.37	0%	5.09	4.16	-18%	CC/CW	CW
2	2FL-C32	2.34	2.62	12%	37.39	46.04	23%	73.40	61.98	-16%	0.65	0.73	12%	10.98	8.60	-22%	CS	CW
3	3FL-C32	3.07	3.27	7%	50.09	49.85	0%	87.70	68.85	-21%	0.86	0.91	7%	13.90	13.32	-4%	CS	CS
4	1FL-C64	2.37	2.42	2%	29.77	38.56	30%	100.80	88.74	-12%	0.66	0.67	2%	6.27	4.16	-34%	CC/CW	TR
5	2FL-C64	3.26	4.83	48%	38.37	47.24	23%	114.50	132.94	16%	0.91	1.35	48%	7.17	8.60	20%	CW	TR
6	3FL-C64	4.62	7.25	57%	35.55	55.34	56%	161.10	161.53	0%	1.29	2.02	57%	15.00	13.32	-11%	CS	TR/CS
7	1FL-C96	3.07	2.42	-21%	35.21	36.79	5%	121.30	94.92	-22%	0.83	0.67	-19%	5.69	4.16	-27%	TR	TR
8	2FL-C96	6.71	4.83	-28%	45.21	43.82	-3%	206.50	146.77	-29%	1.87	1.35	-28%	11.19	8.60	-23%	TR	TR
9	3FL-C96	9.07	7.25	-20%	52.02	50.37	-3%	248.80	181.66	-27%	2.29	2.02	-12%	15.85	13.32	-16%	TR/CS	TR
	Average			6%			15%			-13%			7%			-15%		

Note: Err. = Error (Model vs. Test), CC = Compression Face Crushing, CW = Compression Face Wrinkling, CS = Core Shear, TR = Tension Face Rupture, positive strain = tension, negative strain = compression.

LIST OF FIGURES

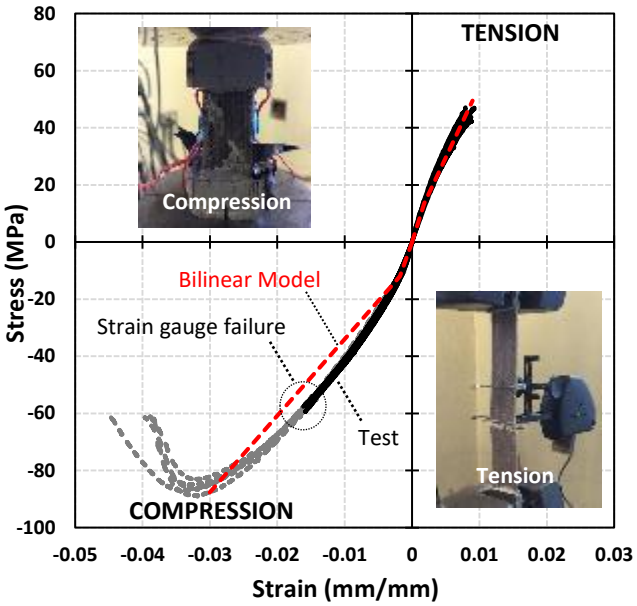

Figure 1: Stress-strain curves of facing materials in tension and compression: coupon tests and proposed bilinear model.

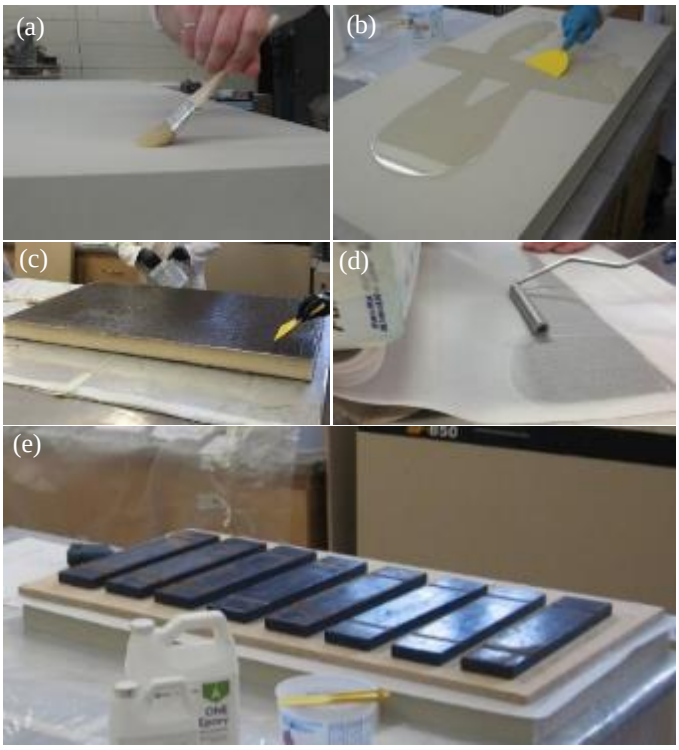

Figure 2: Specimen Fabrication: (a) dust removal; (b) resin application on foam; (c) resin application on flax fabric layer; (d) air removal; and (e) curing.

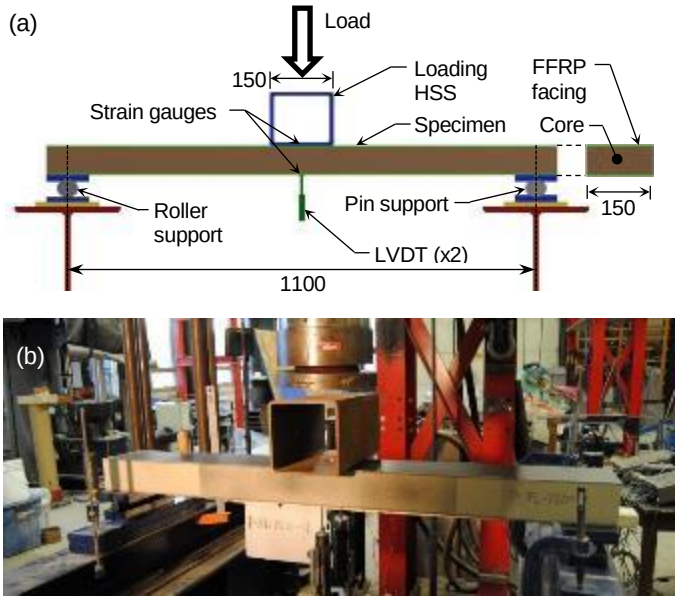

Figure 3: Test set-up and instrumentation: (a) schematic drawing; and (b) photo (dimensions in mm).

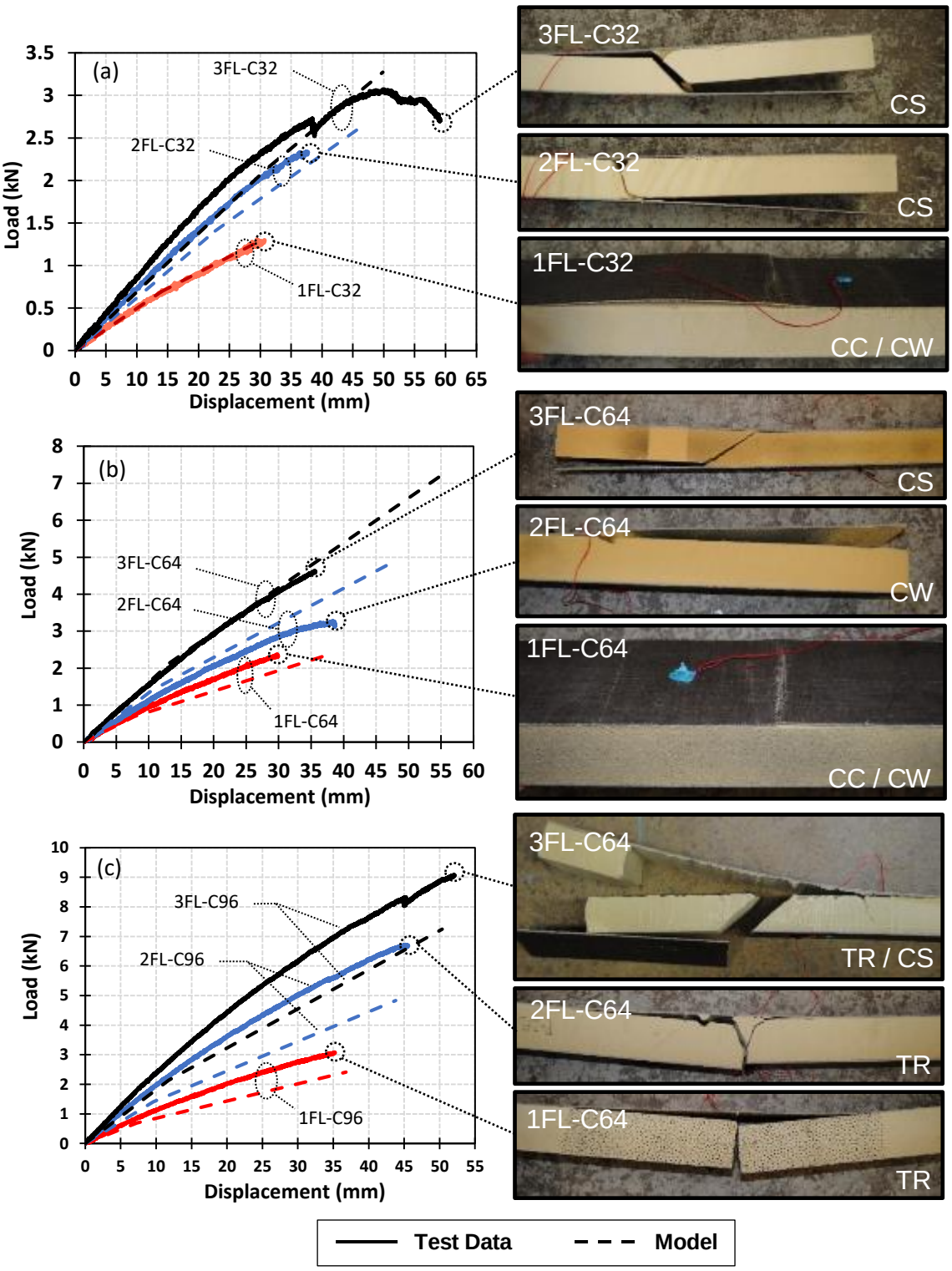

Figure 4: Effect of facing thickness on load-deflection diagrams for different core densities: (a) 32 kg/m^3; (b) 64 kg/m^3; and (c) 96 kg/m^3.

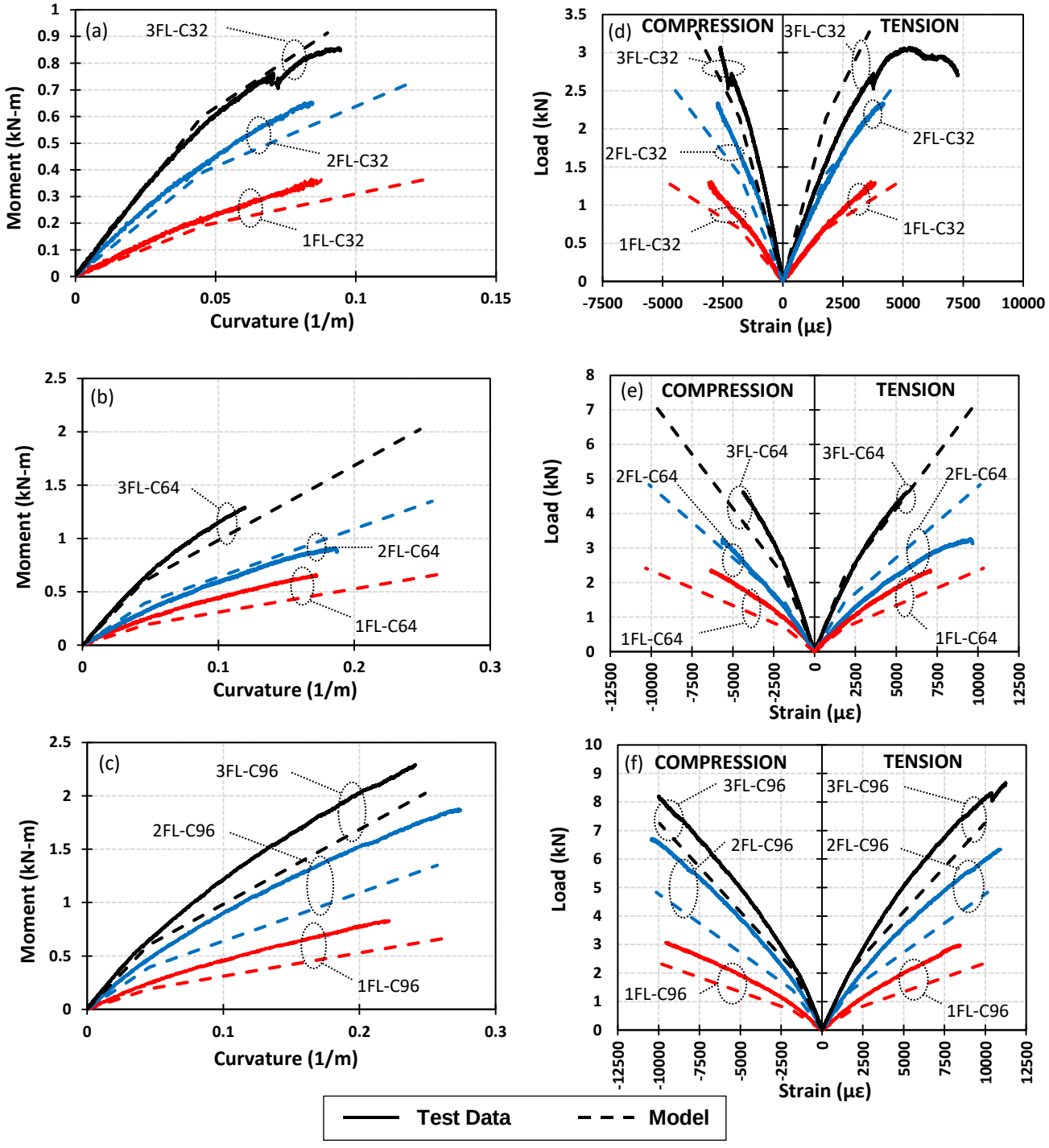

Figure 5: Effect of facing thickness on moment-curvature diagrams for (a) C32; (b) C64; and (c) C96 and load-strain diagrams for (d) C32; (e) C64; and (f) C96.

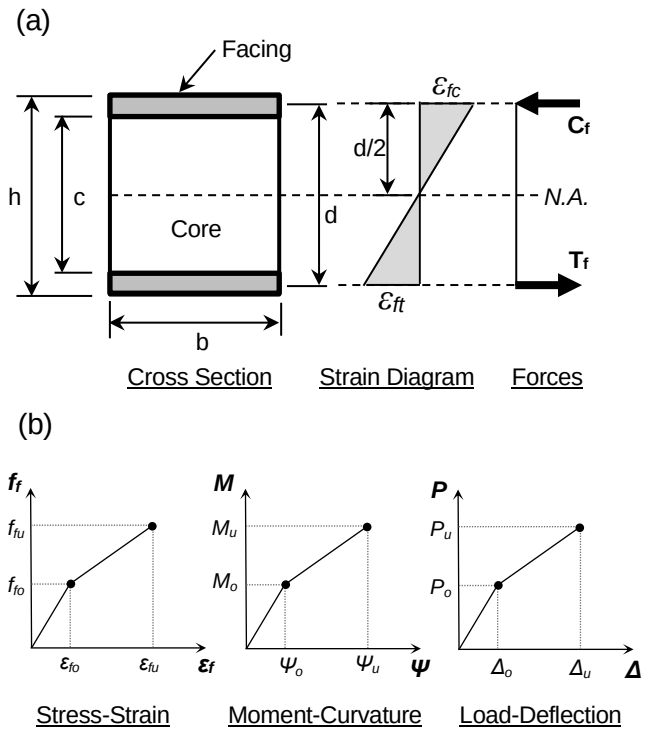

Figure 6: Simplified model: (a) cross-sectional analysis of sandwich panel with FFRP facings; and (b) bilinear stress-strain, moment-curvature, and load-deflection models.

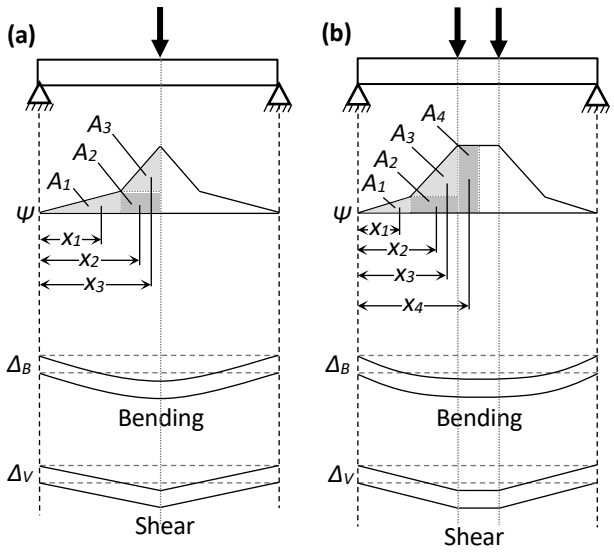

Figure 7: Determinations of deflection through superposition of bending and shear deflections: (a) 3-point bending; and (b) 4-point bending.

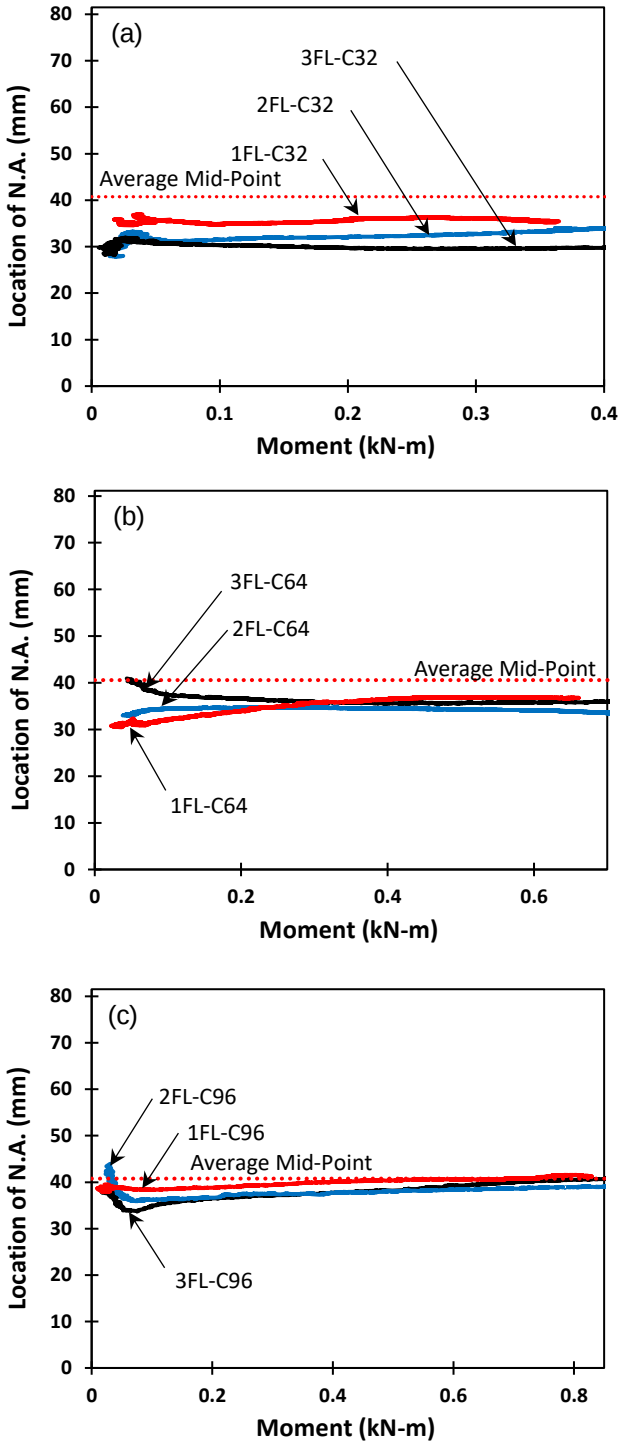

Figure 8: Location of neutral axis vs. moment: (a) C32; (b) C64; and (c) C96.

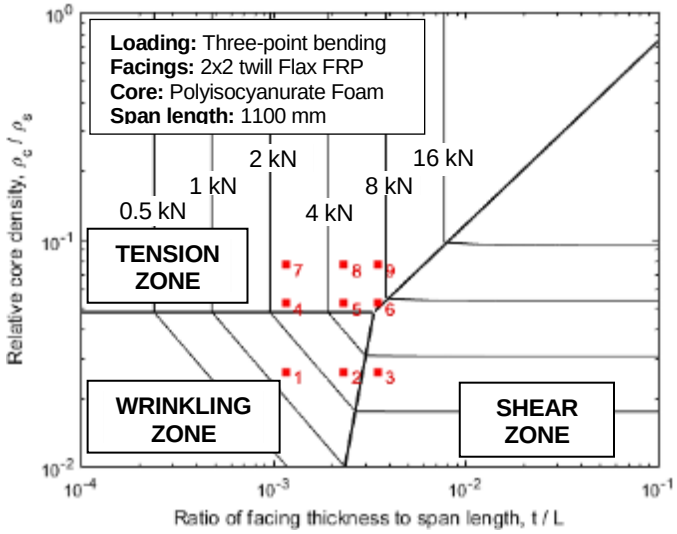

Figure 9. Failure mode map of FFRP-foam sandwich panel (Note: see Table 1 for Specimen Numbers 1 to 9)

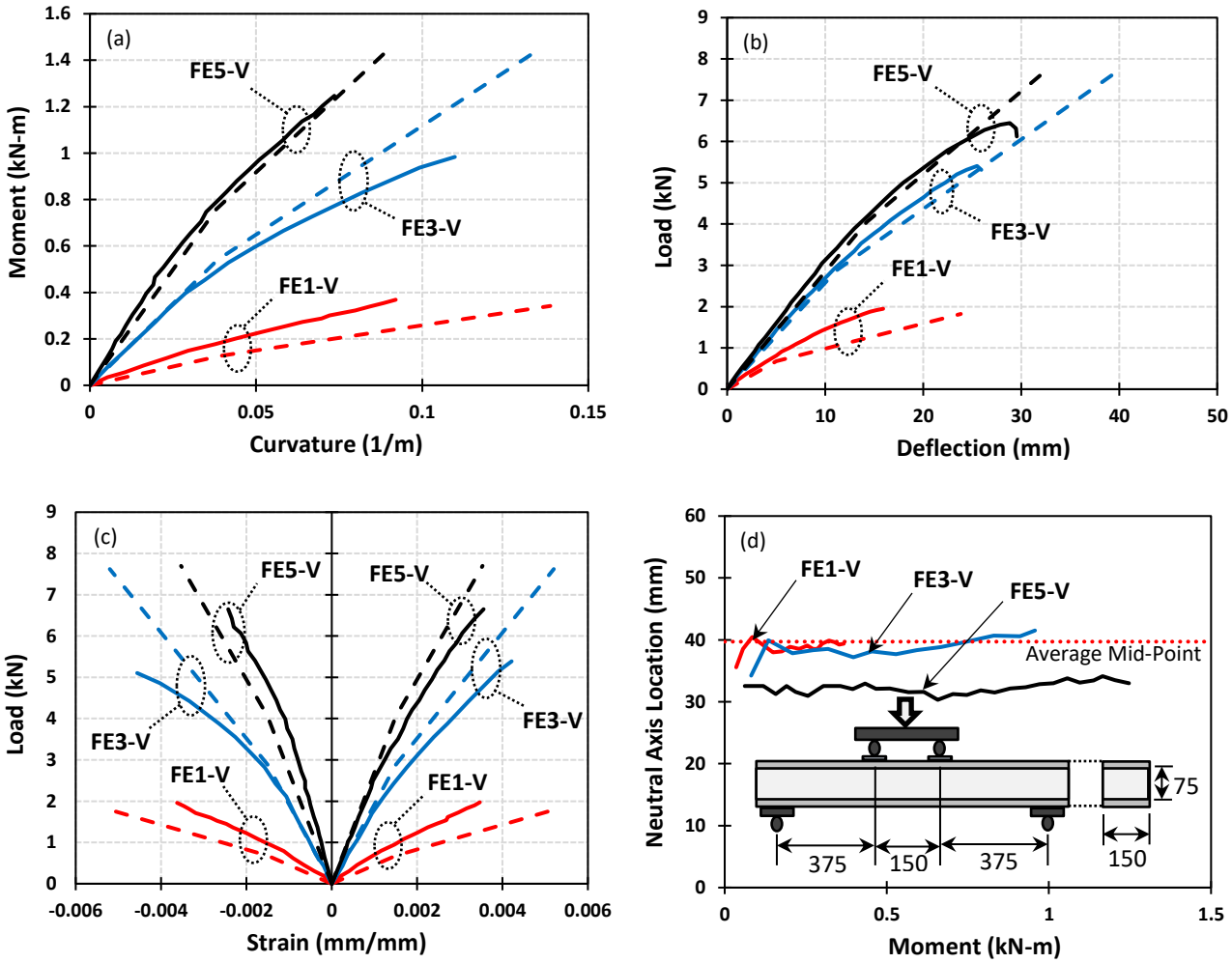

Figure 10: Model verification using test data from Mak et al. (2015): (a) moment-curvature; (b) load-deflection; (c) load-strain; and (d) neutral axis location and test set-up (dimensions in mm).

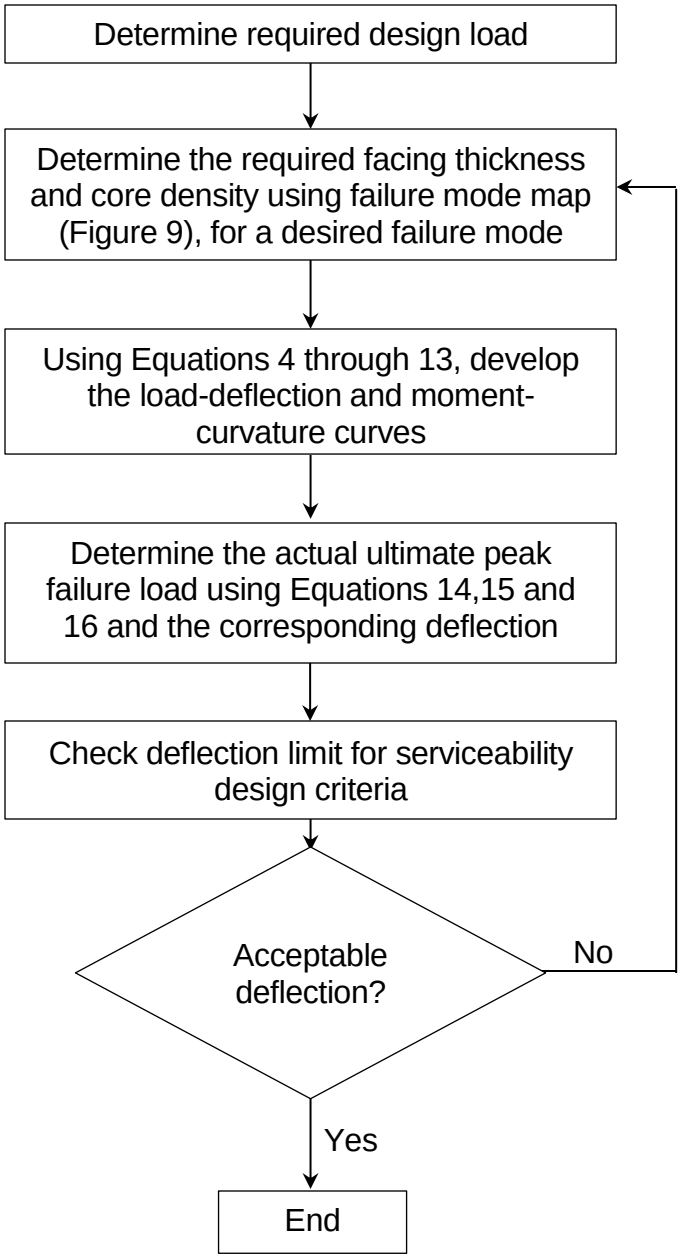

Figure 11. Flow chart for the design of FFRP-foam sandwich beams.